Monthly Notices
of the
ROYAL ASTRONOMICAL SOCIETY

MNRAS **488,** 4858–4872 (2019)
Advance Access publication 2019 July 25

doi:10.1093/mnras/stz1999

Comparing Multiclass, Binary, and Hierarchical Machine Learning Classification schemes for variable stars

Zafiirah Hosenie [1]★ Robert J. Lyon [1] Benjamin W. Stappers[1] and Arrykrishna Mootoovaloo [2]

[1]*Jodrell Bank Centre for Astrophysics, School of Physics and Astronomy, The University of Manchester, Manchester M13 9PL, UK*
[2]*Imperial Centre for Inference and Cosmology (ICIC), Imperial College, Blackett Laboratory, Prince Consort Road, London SW7 2AZ, UK*

Accepted 2019 July 15. Received 2019 July 15; in original form 2019 March 6

ABSTRACT

Upcoming synoptic surveys are set to generate an unprecedented amount of data. This requires an automatic framework that can quickly and efficiently provide classification labels for several new object classification challenges. Using data describing 11 types of variable stars from the Catalina Real-Time Transient Survey (CRTS), we illustrate how to capture the most important information from computed features and describe detailed methods of how to robustly use information theory for feature selection and evaluation. We apply three machine learning algorithms and demonstrate how to optimize these classifiers via cross-validation techniques. For the CRTS data set, we find that the random forest classifier performs best in terms of balanced accuracy and geometric means. We demonstrate substantially improved classification results by converting the multiclass problem into a binary classification task, achieving a balanced-accuracy rate of ∼99 per cent for the classification of δ Scuti and anomalous Cepheids. Additionally, we describe how classification performance can be improved via converting a 'flat multiclass' problem into a hierarchical taxonomy. We develop a new hierarchical structure and propose a new set of classification features, enabling the accurate identification of subtypes of Cepheids, RR Lyrae, and eclipsing binary stars in CRTS data.

Key words: methods: data analysis – methods: statistical – stars: variables: general.

1 INTRODUCTION

Astronomy has experienced an increase in the volume, quality, and complexity of data sets produced during numerical simulations and surveys. One factor that contributes to the data avalanche is the new generation of synoptic sky surveys, for example, the Catalina Real-Time Transient Survey (CRTS; Drake et al. 2017). In addition, the Large Synoptic Survey Telescope (LSST; Ivezic et al. 2008) for example, which is now on the horizon, will produce ∼15 terabyte (TB) of raw data per night (Juric et al. 2015). However, despite this data deluge, source variability is often still visually inspected to detect new promising candidates/variable stars. Visual inspection does have utility for detection and classification. Human experts can extract new useful information despite unevenly sampled data sets and also have the ability to distinguish noisy data from data exhibiting interesting behaviour/characteristics. They can also incorporate complex contextual information into their decision making. However, the efficacy of the manual approach decreases as the volume of data grows exponentially, as will be the case for the next generation of surveys. Visual inspection becomes inconsistent, consequently, mistakes are made, and rare/interesting objects can be missed.

To address this problem, machine learning (ML) has been applied to variable star classification in multiple time series data sets (see Belokurov, Evans & Le Du 2003; Willemsen & Eyer 2007). In ML, variable stars are represented by features: independent measures that contain information useful for differentiating variable stars into their respective classes. Therefore, several developments have been made towards determining the best methods and features for describing variable stars, including the Lomb–Scargle periodogram (Lomb 1976; Scargle 1982), Bayesian evidence estimation (Gregory & Loredo 1992), and hybrid methods (Saha & Vivas 2017). In addition, Eyer & Blake (2005) analysed the small sharp features of light curves and included them as input features to a Naïve Bayes classifier. While Djorgovski et al. (2016) developed an automatic framework to detect and classify transient events and variable stars. They used a subset of the CRTS data to perform classification between two types of variable stars (W Uma and RR Lyrae) and obtained completeness rates of ∼96–97 per cent.

Kim & Bailer-Jones (2016) developed the UPSILON package to classify periodic variable stars using 16 extracted features from

★ E-mail: zafiirah.hosenie@gmail.com

light curves, which achieves good results. Mahabal et al. (2017) developed a classifier based on the convolutional neural network (CNN) model using labelled data sets of periodic variables from the CRTS (Drake et al. 2009; Djorgovski et al. 2011, 2016; Mahabal et al. 2012). They transformed a light curve (time series) into a two-dimensional mapping representation ($dm - dt$) that is based on the changes in magnitude (dm) over the time difference (dt). Using multiclass classification, their algorithm achieved an accuracy of ∼83 per cent. Narayan et al. (2018) developed an ML approach to classify variable versus transient stars. Similarly, they performed a multiclass classification of combined variable stars and transients, and a 'purity-driven' subcategorization of the transient class using multiband optical photometry. Revsbech, Trotta & van Dyk (2018) used a data augmentation technique to mitigate the effects of bias in their data by generating additional training data using Gaussian processes (GPs). They used a diffusion map method that calculates a pairwise distance matrix that outputs diffusion map coefficients of the light curves. These coefficients act as feature inputs to a random forest (RF) classifier used to help identifying Type Ia supernova.

We found that it is fundamentally important to develop accurate and robust automated classification methods for this problem using ML and other statistical approaches. This paper describes a new automatic classification pipeline for the classification of variable stars via application to archival data. To our knowledge, this is the first time the southern CRTS (Drake et al. 2017) data set has been used to build/evaluate an automatic classification system.

Similar work has been completed in recent years (Kim & Bailer-Jones 2016; Mahabal et al. 2017; Narayan et al. 2018), though the features used for learning are rarely evaluated in a statistically rigorous way. We found that using a large set of features does not imply higher classification metrics. We therefore perform an in-depth analysis of ML features to understand their information content, and determine which give rise to the best classification performance. We utilize various visualization techniques and the tools of information theory to achieve this.

Based on our analyses we find that accurate variable star classification is possible with just seven features – much fewer than in other works. In addition, we show that this classification problem cannot be solved with a 'flat' multiclass classification approach, as the data are inherently imbalanced. To partially alleviate the 'imbalanced learning problem' (Last, Douzas & Bacao 2017), we developed an approach inspired by earlier work in this area (Richards et al. 2011). This involved converting a standard multiclass problem in to a hierarchical classification problem, by aggregating subclasses in to superclasses. This results improved performance on rare class examples typically misclassified by multiclass methods. We adopt a similar methodology to Richards et al. (2011), however we (i) propose a different hierarchical classification structure, (ii) use a different feature analysis/selection methodology resulting in different feature choices, (iii) apply hyperparameter optimization to build optimal classification models, and finally (iv) apply the resulting approach to CRTS data.

The outline of this paper is as follows. In Section 2, we provide a brief description of the data set used and in Section 3, we present the feature generation techniques we employ here; while in Section 4, we explain how we build the classification pipeline. In Section 5, we apply state-of-the-art feature visualization techniques to visualize how separable our features are before performing a multiclass classification. In Section 6, we provide an in-depth feature evaluation to determine the usefulness of our extracted features before performing a binary classification. In Section 7, we present a hierarchical taxonomy for classification and discuss our results; finally, we summarize our results and conclusions in Section 8.

2 DATA

We use the publicly available CRTS (Drake et al. 2017) data set that covers the sky with declinations between −20° and −75°. The sources in the data set have median magnitudes in the range $11 < V < 19.5$. The data set contains different forms of periodic variable stars, these are stars that undergo regular changes in brightness every few hours or within a few days or weeks. The periodic variable stars in the data set can generally be classified into three broad classes: namely eclipsing, pulsating, and rotational. The classes can be further divided into subtypes, for example pulsating stars consist of δ Scutis, RR Lyrae, Cepheids, and the long-period variables (LPVs) group that includes both semiregular variables and Mira variable stars. The RR Lyrae class consists of RRab's (fundamental mode), RRc's (first overtone mode), and RRd's (multimode). However, many RR Lyrae stars are known to exhibit the Blazhko effect (long-term modulation; Blazhko 1907). In addition, the Cepheids include Type II Cepheids (Cep-II), anomalous Cepheids (ACEPs), and classical Cepheids. The eclipsing binary variables in the data are divided into detached binaries (EA) and contact plus semidetached binaries (Ecl). The rotational class consists of variable stars including the ellipsoidal variables (ELL) and spotted RS Canum Venaticorum (RS CVn) systems. A more detailed overview of the data set is given in Drake et al. (2017) and Catelan & Smith (2015) gives a more detailed overview of the properties of the various types of pulsating stars.

The data set contains about 37 745 periodic variable stars (Catalina Surveys Data Release 2,[1] CSDR2). For our analysis, we use a sample of 37 437 out of the 37 745 stars from the CSDR2. We have excluded Type 11: miscellaneous variable stars (periodic stars that were difficult to classify as presented in Drake et al. 2017), and Type 13: LMC-Cep-I that as a group consists of only 10 examples. We remove the smallest classes as there are too few samples to characterize those classes, as we also know that classifiers given such data will struggle to categorize them accurately due to the imbalanced learning problem (Last et al. 2017). Furthermore, we downsample Type 5: semidetached binary stars to 4509 samples as this class of object originally consisted of 18 803 samples. We perform this downsampling to prevent the large class from dominating the training sets, which could otherwise potentially bias a classifier. The excluded samples of Type 5 are then included in the test set. Fig. 1 shows examples of folded light curves for each class under consideration. We also present the number of samples considered for the 11 different types of variable stars in Fig. 2. Note that ∼14 294 samples of Type 5: Ecl, unused during training, were eventually used in the test set.

3 FEATURE GENERATION

In general, ML algorithms use training data to build a mathematical model, where the training data are composed of feature data. These features may have varying utility, i.e. information-rich features are desirable as they can be used to build more accurate classification systems. In this work, we generate statistical features from the light curves to characterize and distinguish different variability classes. Let $S = \{X_1, \ldots, X_n\}$ represents the set of variable star

[1] Catalina Surveys Data Release 2.

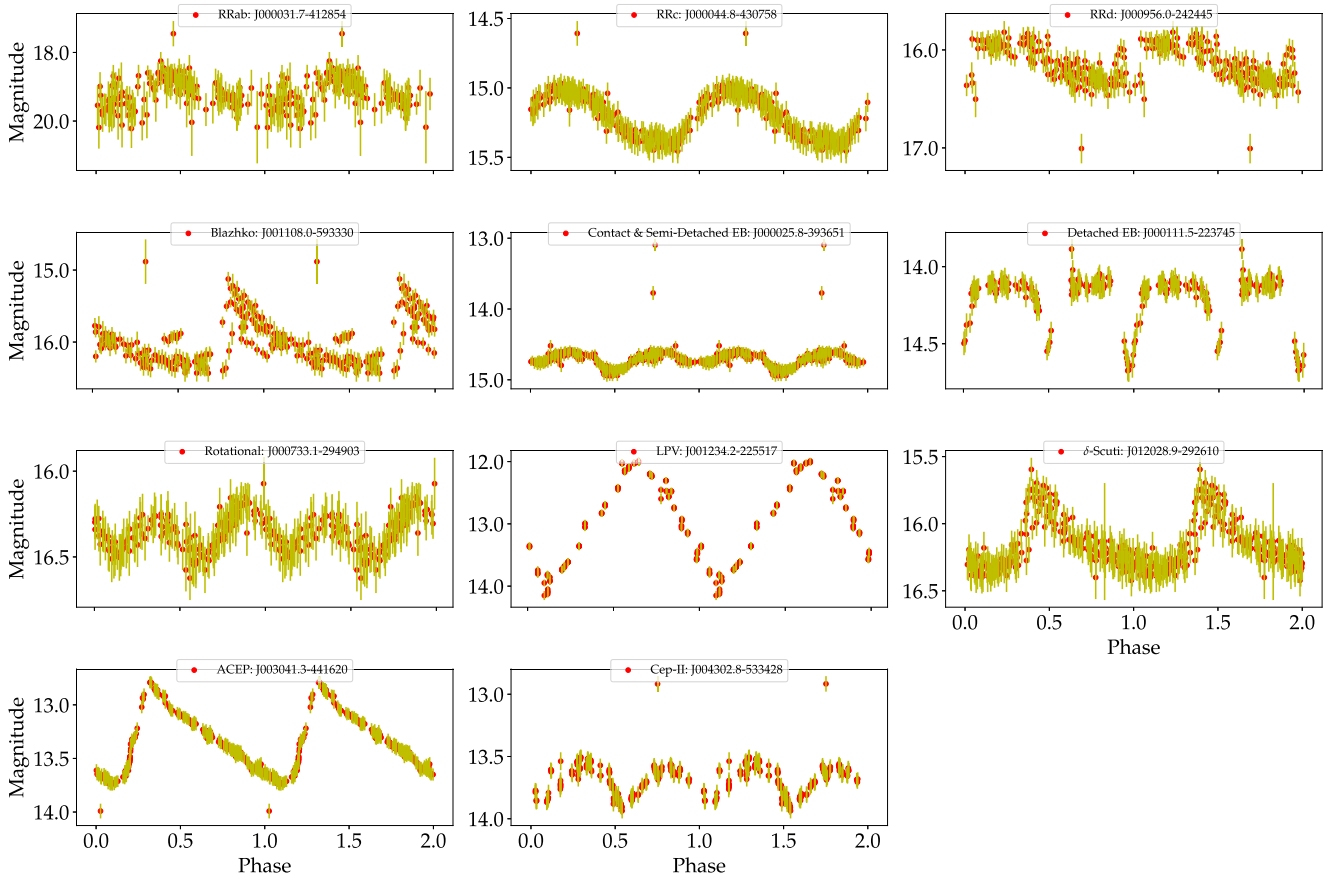

Figure 1. Examples of folded light curves from the CRTS for the various types of variable stars considered in our analyses.

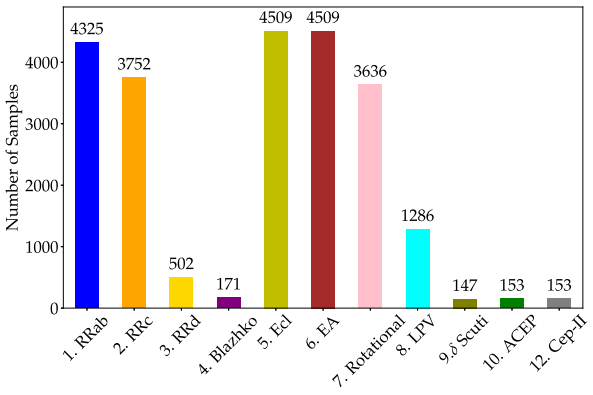

Figure 2. Class distributions for the CSDR2 data sets. We downsample Type 5: semidetached binary stars to 4509 samples to prevent larger classes from dominating the training sets. The excluded samples ∼14 294 for Type 5: Ecl are then included in the test set for prediction. These distributions highlight the remaining imbalance in the data sets.

data available to us, then X_i is an individual star represented by variables known as *features*. An arbitrary feature of star X_i is denoted by X_i^j, where $j = 1, \ldots, l$. Each variable star has an associated label y such that $y \in Y = \{y_1, \ldots, y_k\}$. For multiclass scenarios the possible labels assignable to variable stars vary as $1 \leq y \leq 12$ but since we do not consider Type 11 examples for reasons given at the end of Section 2, we note that $y \neq 11$. Meanwhile for binary class classification scenarios, we consider binary labels $y \in Y = [0, 1]$.

The goal is to build a ML algorithm that learns to classify variable stars described by features, from a labelled input vector, also known as the training set, $X_{\rm Train}$. The training set consists of pairs such that $X_{\rm Train} = \{(X_1, y_1), \ldots, (X_n, y_n)\}$. The learnt mapping function between input feature vectors and labels in $X_{\rm Train}$ can then be utilized to label new unseen stars in $X_{\rm Test}$.

In this work, we focus mainly on using the statistical properties of the data with no preconceived notions of their suitability or expressiveness as input features to our ML algorithms. As a result we focus on seven features, of which six are intrinsic statistical properties relating to location (mean magnitude), scale (standard deviation), variability (mean variance), morphology (skew, kurtosis, and amplitude), and time (period). These features are highly interpretable, and robust against bias. Note that we remove data points from light curves that are 3σ above or below the mean magnitude, where σ is the standard deviation and it is an important step to remove any outliers in the data. This cleaning does not alter the light curves significantly as it removes less than 1 per cent of their data points.

Afterwards, we used the FATS[2] (Nun et al. 2015) PYTHON library to extract these features. FATS takes as input the unfolded light curves and it outputs various statistical features: the mean, standard deviation, skew, kurtosis, mean variance, and amplitude. We also incorporate the period for each star given in the catalogue as a feature to our ML algorithms. The description of the input features used for

[2]FATS: Feature Analysis for Time Series.

Table 1. The seven features used as inputs to our classification scheme. Six features based on simple statistics are extracted directly from light curves using FATS. Note that the period feature is obtained from the Drake et al. (2017) catalogue.

Features	Description	Symbol
Mean	$\mu = \frac{1}{N}\sum_{i=1}^{N} m_i$, where m is the magnitude and N is the number of data points	μ
Standard deviation	$\sigma = \sqrt{\frac{1}{N-1}\sum_{i=1}^{N}(m_i-\mu)^2}$	σ
Skewness	$\gamma = \frac{N}{(N-1)(N-2)}\sum_{i=1}^{N}\left(\frac{m_i-\mu}{\sigma}\right)^3$	γ
Kurtosis	$\text{kurt} = \frac{N(N+1)}{(N-1)(N-2)(N-3)}\sum_{i=1}^{N}\left(\frac{m_i-\mu}{\sigma}\right)^4 - \frac{3(N-1)^2}{(N-2)(N-3)}$	kurt
Mean variance	This is a simple variability index and is defined as the ratio of the standard deviation, σ, to the mean magnitude, μ	$\frac{\sigma}{\mu}$
Period	Drake et al. (2017) used the Lomb–Scargle (L–S) periodogram analysis together with an adaptive Fourier decomposition (AFD) method to calculate the period of unevenly sampled data. More information about this feature can be found in Drake et al. (2017)	T
Amplitude	The amplitude is half of the difference between the median of the maximum 5% and the median of the minimum 5% magnitudes	Amp

classification is listed in Table 1. Practitioners should be cautious when applying the mean magnitude as a feature in combination with data obtained at another telescope. It has the potential to bias a training set against fainter/brighter sources. We note that adding the telescope label as a feature may overcome this issue, but we leave that to future work.

One important aspect of the training process used to build a classification model is data pre-processing. Some ML algorithms, e.g. functions/classifiers that calculate the distance between data points, will not work properly without normalization or standardization since the range of values of the features/raw data varies widely. We therefore employ a normalization method, $\hat{\mathbf{S}}$, to standardize the feature data such that all values in the feature space are scaled between 0 and 1.

4 CLASSIFICATION PIPELINE

In this section, we describe the process used to perform the classification of variable stars, for instance, training, hyperparameter optimization, and prediction. We first extract features and then split the feature data into the training (70 per cent) and the test (30 per cent) data. The training data are used to train the model while the test data are used to evaluate the performance of the trained model. Once the data are split into two, we perform a simple normalization where each feature X_i^j is divided by its maximum, $\max(X_i^j)$ (see equation 1). The goal of normalization is to ensure that all features use a common scale. This is beneficial for ML algorithms that are sensitive to feature distributions, for instance, distance-based algorithms that require Euclidean distance computation (e.g. k-nearest neighbours, kNN). Some models [e.g. decision tree (DT), RF] are less sensitive to feature scaling. However, it is good practice to standardize when comparing between classification systems to rule out potential sources of disparity in our results. Note that in this context, we found that this simple normalization was enough to yield good performance. For X_{Test}, the features are then rescaled using $\max(X^j_{\text{Train}_i})$,

$$X_{\text{Train}} = \left|\frac{X_{\text{Train}_i}}{\max\left(X_{\text{Train}_i}\right)}\right|, \qquad X_{\text{Test}} = \left|\frac{X_{\text{Test}_i}}{\max\left(X_{\text{Train}_i}\right)}\right|. \tag{1}$$

Afterwards, we apply some feature evaluation strategies to check whether the features show some separability. Then, for our classification purposes, we apply three different classification algorithms: DT, RF, and kNN, accomplished with Scikit–Learn (Pedregosa et al. 2011). kNN (Buturovic 1993) is a simple instance-based technique that assigns an unlabelled example, the label of its k nearest neighbours. This method is based on the Euclidean distance measure. kNN performs effectively when the training data set is sufficiently large. However, one disadvantage of kNN is that all the features are needed when computing the distance between data points. If a small portion of the data set consists of discriminatory information and the larger portion contains irrelevant features, the distance between the instances will be more influenced by the irrelevant samples and their feature values.

In contrast, DTs (Quinlan 1986) attempt to split input data recursively according to feature values. Each split creates a branch, and there can be arbitrarily many branches in a tree. Each branch eventually terminates at a leaf node that is associated with a specific label. The goal of tree learning is to build a tree structure that has decision paths (from tree root to leaf nodes) that accurately separate examples moving down the tree so that they arrive at the correct leaf node (i.e. obtain the correct label). Generally, using a single decision tree for classification often leads to poor performance due to low or high variance. For instance, a small change in the training set can lead to a very different learned tree structure. Given the weakness of individual trees to training variance, multiple trees can be combined to overcome this problem. Any method that combines multiple single-model classifiers in this manner is known as an ensemble method (Dietterich 2000). For instance, an RF (Breiman 2001) is simply an addition of decision trees that aggregate tree decisions, usually leading to improved classification performance. Such ensemble methods have been shown (Richards et al. 2011; Lochner et al. 2016; Narayan et al. 2018) to achieve better results than single-model learners on a variety of data sets.

A major problem faced when using various classifiers is hyperparameter optimization. This is crucial for finding the hyperparameters that yield the best overall classification performance for a specific problem. The most widely used techniques are HYPEROPT (Bergstra, Yamins & Cox 2013), a Bayesian optimization approach, grid search, and manual search. In our study, we adopt a randomized search that iterates a number of times through pre-specified hyperparameters and finds the optimum parameter that outputs the best balanced accuracy for a classifier. Together with the randomized grid search for hyperparameter optimization, we apply fivefold stratified cross-validation (see Section 4.1) on the training set to evaluate

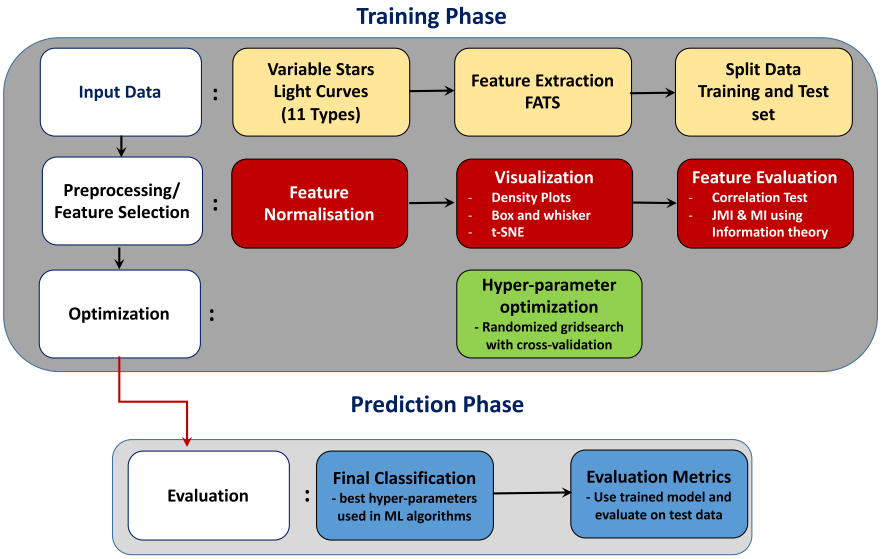

Figure 3. The different stages of our classification framework. First, we use light curves of variable stars as input data. For the first stage process, features are extracted using FATS and then are later split into training and test sets. The second stage involves data pre-processing and feature selection. In this process, the extracted features are normalized, visualized, and selected based on various techniques. Afterwards, the third stage covers hyperparameter optimization using the randomized grid search with cross-validation methods. Finally, the last stage uses the best hyperparameter to re-train the ML algorithms using the entire normalized training set in stage 2 and evaluate it on the normalized test set in stage 2 using various metrics to quantify the models.

model performance, i.e. the 70 per cent training set is further split into training and validation sets. We cross-validate to ensure any observed results are real and not just due to some data set specific effect. We note that CRTS data exhibit distributional disparities – some types of star are common in the data, while others are relatively rare. Traditional ML classifiers perform poorly on such data (He & Garcia 2008). They become biased towards correctly classifying the common classes, a strategy that typically yields the greatest overall accuracy. In some cases, this bias can be overcome by re-weighting training examples so that rare examples are weighted higher than common ones. However where/when imbalance is manifested via complex data characteristics (class overlap, small disjuncts, subclass inseparability; see He & Garcia 2008), re-weighting alone is insufficient. Based on our analysis of our data presented in Sections 5.1 and 5.2, we see enough imbalanced characteristics to suggest that our problems cannot be solved by weighting alone, none the less we apply re-weighting with the aim of mitigating such problems.

We then proceed with cross-validation, use the best model hyperparameters found during this process and re-train the model with the entire 70 per cent training set. The trained model is then evaluated on the test set (30 per cent), $X_{\rm Test}$, using various evaluation metrics described in Appendix A. The performance of our pipeline is evaluated on balanced accuracy, the geometric mean (G-mean) score, F1-score, recall, and standard confusion matrices. The classification pipeline is summarized in Fig. 3.

4.1 *K*-fold cross-validation

When using ML algorithms, another major problem is an overoptimistic result, i.e. the output results are too good to be true on training data, due to over/underfitting. Overfitting mostly happens when we perform training and evaluation on the same data. Therefore, classification algorithms must be tested on independent data to avoid this problem. One method for avoiding this involves splitting the data into training and testing sets as explained in Section 3. Another common method for splitting data sets for evaluation is known as *K*-fold cross-validation, i.e. the training data set S is split randomly into K mutually exclusive subsets $(S_1, S_2, \ldots, S_K)$ of nearly the same size. The classification algorithm is trained and tested K times. For each time step $t \in \{1, 2, \ldots, K\}$, the algorithm is trained on $K - 1$ folds and one fold S_t is used for validation. In addition, a stratification of the data is applied such that for each of the $K -$ folds, the data are arranged to ensure each fold preserves the percentage of samples for each class in the data set at large. The overall balanced accuracy of an algorithm trained/tested via cross-validation is simply the average of each of the K balanced-accuracy measures obtained after each time step.

5 MULTICLASS CLASSIFICATION

Our main goal is to perform a multiclass classification using our classification pipeline previously described. We first apply some feature evaluation strategies to check whether our extracted features in Section 3 are good for classification. The most common methods that characterize 'good' features: look for the presence of linear correlations between the features and the class labels, and/or we sometimes indirectly measure feature utility by using classification performance (e.g. Bates et al. 2011) as a proxy. If performance is good, we assume the features have utility. However, it is often misleading to evaluate features based on classifier performance as it varies according to the classifier used (Brown et al. 2012).

In this work, we employ the three primary considerations as in Lyon et al. (2016) to evaluate our features. A feature must (i) show importance in discriminating between the different classes/types of variable stars, (ii) maximize the separation between the various variable stars, and (iii) lastly yield a good performance when used in conjunction with a classification algorithm. We have therefore applied two feature visualization strategies

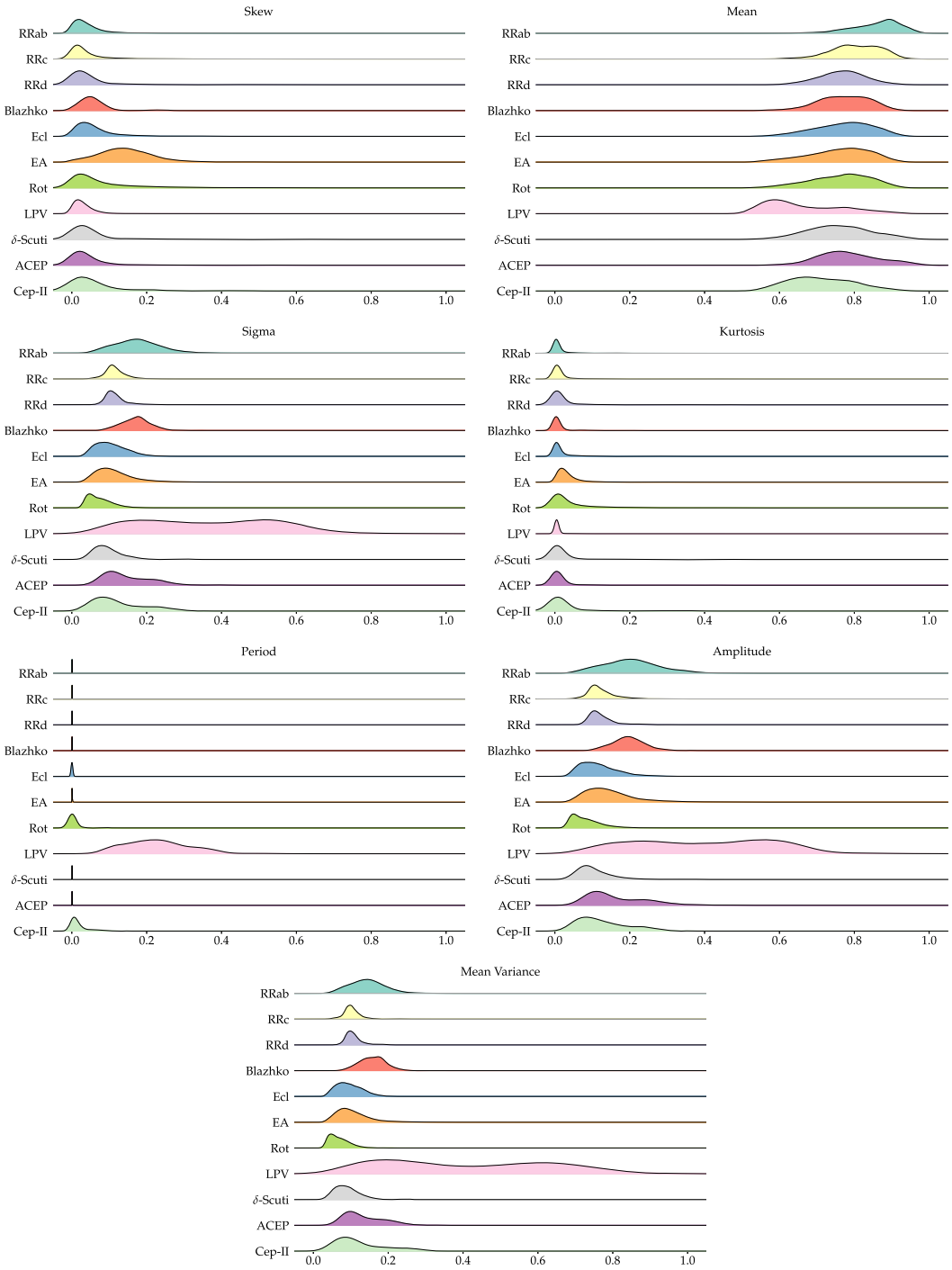

Figure 4. One-dimensional density estimates of the selected features by class. The features considered are (a) skew, (b) mean, (c) sigma, (d) kurtosis, (e) period, (f) amplitude, and (g) mean variance.

to our features given in Table 1 before performing a multiclass classification.

5.1 Visualization of feature space with one-dimensional density estimates

One way to visualize the features we extracted in Section 3 is to plot one-dimensional density estimates of the observed distribution as shown in Fig. 4. This plot allows us to visually compare the distributions of the normalized features for the different classes of variable stars. The plots depict distinct feature-by-feature characteristics of each class. It enables us to identify outliers and determine if there is multimodality in the feature space. For example, the RR Lyrae skew distributions are mostly narrow and peaked, showing that these classes are well characterized by the skewness. In addition, the density plots provide us with information of which features are fundamentally important in discriminating different sets of classes. Some classes have overlapping distributions for one or more feature

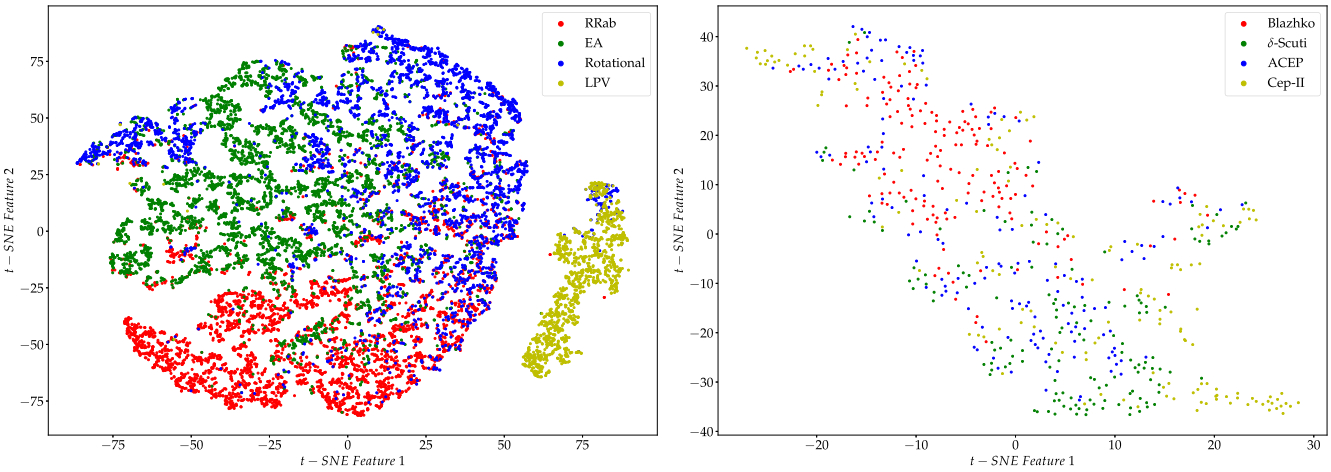

(a) t-SNE with large sample data

(b) t-SNE with small sample data

Figure 5. (a) Shows the t-Distributed Stochastic Neighbour Embedding (t-SNE) visualization for the feature set after normalization with large sample data (RRab, EA, rotational, and LPV). We note that the classes are quite well separated in the embedding space. (b) Illustrates t-SNE visualization for the feature set after normalization with the small sample size data (Blazhko, δ Scuti, ACEP, and Cep-II). No distinct separation is seen within the small sample data set.

variables. This applies to the RR Lyrae, eclipsing binary, and the Cepheid stars. Whilst other classes, such as the LPVs have trivially separable distributions, suggesting that the LPV class should be easy to classify. However, more rigorous investigation is needed to determine with confidence whether these features are useful for classification purposes.

5.2 t-SNE

After visualizing the individual features separately, we wish to understand the relationship between our features but this is difficult to do given the feature dimensionality we are dealing with. Yet it is possible to overcome this problem by reducing the dimensionality so that it is representable in a 2D or 3D representation space. t-Distributed Stochastic Neighbour Embedding (t-SNE; van der Maaten & Hinton 2008) is a tool for performing this reduction and visualization.[3]

More specifically, similar objects in high-dimensional space are clustered together with nearby points using a *k*-d tree (Bentley 1975) of all the points. Using a Student's *t*-distribution (same as the Cauchy distribution; Cauchy 1853), the Euclidean distance between each point and its *k*NN is computed. This distance is further converted into a probability distribution. Similar points have a high probability of being assigned to the same class and different points have a low probability of being picked. Afterwards, t-SNE constructs a similar probability distribution using a gradient descent method, in the low-dimensional space over the points, thus minimizing the Kullback–Leibler divergence between the two probability distributions (Kullback & Leibler 1951).

Generally, classes that are well separated in a t-SNE visualization yield good levels of classification performance by ML systems. However, the converse is not strictly true (Lochner et al. 2016). We use t-SNE only for the visualization of class separability as there are various limitations with t-SNE, as neither the sizes of the clusters nor distance between the points may be informative (Wattenberg, Fernanda & Johnson 2016). For our high-dimensional visualization, we partition the data into two categories: (i) data with large sample sizes that consist of RRab, RRc, Ecl, EA, rotational, and LPV stars; and (ii) data with a small sample size containing RRd, Blazhko, δ scuti, ACEP, and Cep-II. Fig. 5(a) shows quite well-separated classes for the large sample sizes and we would expect our ML algorithms to perform well using this data. Fig. 5(b) strongly suggests inseparability of the classes for the small sample data. This inseparability may be attributed to the fact that there are few examples of each class. Also, another possible explanation is that, for these stars, other features might be required to enable separability. After performing some feature visualization, we decided to use all of the features as inputs to perform a multiclass classification.

5.3 Performance of multiclass classification

We implement three classifiers, RFs, DTs, and *k*NN, to perform an 11-class classification. Of these, RF achieves the best performance with a balanced-accuracy rate of ∼70 per cent on the 30 per cent test data. This poor performance is not surprising, given the large class imbalance present in the data, i.e. the classes with small sample sizes make up just ∼6 per cent of the whole data set. The results presented here are mainly focused on the RF classifier as this achieves the best performance balanced accuracy. In Fig. 6, we plot the confusion matrix of the RF classifier that depicts the predicted class versus the true class in a tabular form. The results obtained by a perfect classifier would result in values only along the diagonal of the confusion matrix. The off-diagonals give us information about the various types of errors that the classifier makes.

We note that some of the mistakes made by the classifier can be attributed to the fact that some of the science classes are physically similar, for example, the RR Lyrae, eclipsing binaries, and Cepheids subclasses. We also note that most of the misclassified examples arise from classes for which there are few training examples, hence indicating bias toward larger classes, which illustrates that class imbalance is an issue. Classes comprising many examples are more likely to be correctly classified, implying that having more examples of the under-represented science classes will help the classification.

[3] sklearn.manifold.TSNE

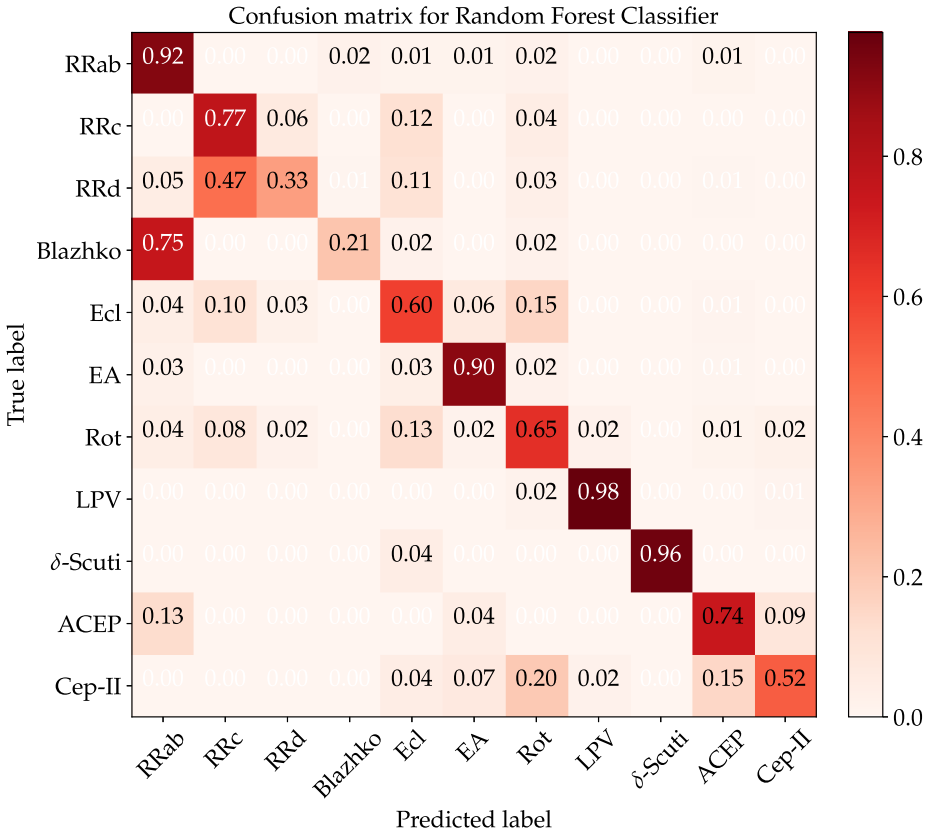

Figure 6. Normalized confusion matrix for multiclass classification with the RF classifier using the best hyperparameters from a randomized grid search cross-validation. The RF classifier was applied on a 70 per cent training set and evaluated on a 30 per cent test set. The classifier performs poorly on under-represented class labels.

6 BINARY CLASSIFICATION

Given the complication of the multiclass classification scheme, decomposing the multiclass problem into smaller binary class problems may alleviate this issue. This may reduce the higher complexity inherent to an 11-class problem. Therefore, in this section we consider binary cases for the classification scheme.

In addition, the poor performance of the multiclass classification in the previous section can be attributed not only to class imbalance but also to the relative importance of features. Therefore, to further investigate whether the features we used are important for classification, we perform an in-depth analysis of the features used for binary classification in Sections 6.1–6.3 by using roughly balanced classes. Feature selection strategies can be grouped in various categories: classifier independent (filter methods) and classifier dependent (wrapper and embedded methods) are the most common. Whilst it is possible to evaluate feature importance using some classification models (e.g. using a RF), we instead decouple feature analysis from any specific classifier model. We do this as wrapper methods are susceptible to overfitting, which can lead to feature choices that may not generalize well beyond the classifier used during selection (Brown et al. 2012). Thus in this paper, we used mostly filter methods. These methods rank the features based on statistical measures of information content, determined by calculating the correlations/relationships between them.

Recall that in Section 5.2, we subdivided the data set into two subsets, namely small and large samples, for which each has roughly equal number of examples. We therefore consider pairwise combinations of each class within the small-sample data set and perform feature selection and binary classification. This is repeated for the large-sample data set. Here, we report on results for Type 1 (RRab) and Type 6 (EA) only for in-depth feature analyses. However, similar performance is obtained for the other pairwise combinations. For the performance of binary classification, we report the results obtained with Type 1 (RRab) and Type 6 (EA) from the large sample data set and Type 9 (δ Scuti) and Type 10 (ACEP) from the small-sample data set.

6.1 Data visualization for binary classes

The discriminating capabilities of the features are examined for some binary cases. To determine if there is some amount of separability between the two classes, we plot the box and whisker plots for the different features extracted. The data have been pre-processed by performing the normalization described in Section 3. Here, we take Type 1 (RRab) as the negative class and Type 6 (EA) as the positive class. For each individual feature, the median value of the negative class is subtracted. This ensures a fair separability scale and centres the plots around the median, hence a distinct separation is seen more clearly between the two classes. The box plots centred on the median value represent the feature distribution of the negative class. Fig. 7 shows a reasonable amount of separability between Type 1, RRab, and Type 6, EA. For each individual feature, we note a clear separability between the two classes, except for the period T. At this point, we are tempted to write-off this feature,

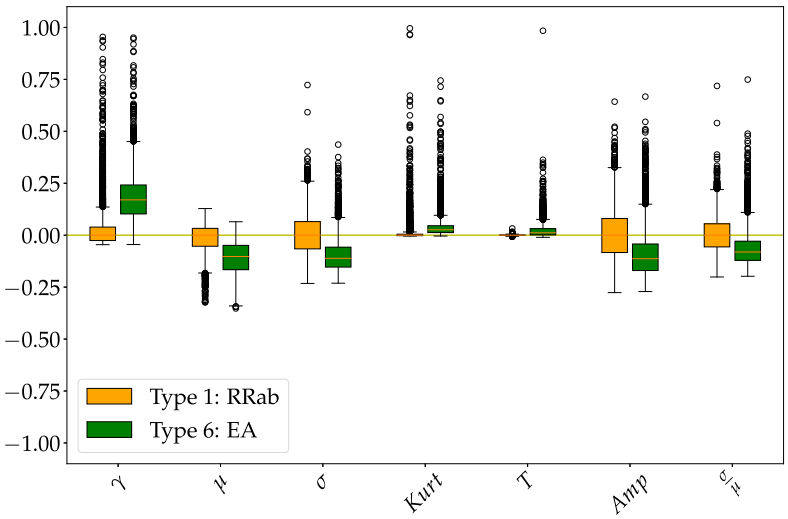

Figure 7. The box and whisker plots show how the features separate RRab (Type 1) and EA (Type 6) examples. The orange coloured boxes describe the feature distribution for RRab sources, where the corresponding black circles represent extreme outliers. The box plots in green describe the EA distributions. There is no clear separation of the period (T) between the two classes. The other features show varying degrees of improved separability, and are generally easily separable at a visual level between the two different types. Refer to Table 1 for definitions of the features used.

Table 2. The point biserial correlation coefficient and the mutual information MI(X; Y) for each feature for the binary class pair: RRab (Type 1) and EA (Type 6) are illustrated. Higher mutual information is desirable. A high MI value implies that there is a strong correlation between the features and the class labels. In addition, the joint mutual information (JMI) rank is given for each feature. A lower JMI rank is preferred. The JMI ranking illustrates the importance of each feature after taking into account the redundancy between features.

Features	Classes Type (1 and 6)		
	r_{pb}	MI	JMI
Skew	0.648	0.503	2
Mean	−0.547	0.260	6
Std	−0.481	0.402	4
Kurtosis	0.248	0.486	3
Period, T	0.019	0.336	1
Amplitude	−0.375	0.307	5
Mean variance	−0.368	0.174	7

however, for a more rigorous analysis of feature selection, we extend our investigation by looking for any linear correlation between the features and the class label.

6.2 Point biserial correlation test

The point biserial correlation coefficient, r_{pb} (Gupta 1960), is applied to find the relationship between a continuous variable, x, and binary variable, y. Similarly to other correlation coefficients, it varies between −1 and +1, where +1 corresponds to a perfect positive relation and −1 corresponds to a perfect negative relation, while a value of 0 means there is no association at all. The point biserial correlation coefficient is similar to the Pearson product moment (Pearson 1895). More detailed information can be found in Lyon et al. (2016).

Table 2 illustrates the correlation between the seven features studied and the target class variable, for one binary class. From Table 2, it is observed that there are three features that show strong correlations ($>\|0.45\|$), for instance, the skew, the mean, and the standard deviation. It can also be seen from Table 2 that the T exhibits a weak correlation for this binary class pair. This means that T might not be useful for classification. However, again one should be careful when judging the feature importance based upon their linear correlations. Features having linear correlations close to zero, may have useful non-linear correlations.

6.3 Information theory

To investigate the relative importance of the features, we implement the information theoretic method that Lyon et al. (2016) applied to the pulsar search problem. According to Guyon & Elisseeff (2003), features that appear to be information poor, may provide new and meaningful information when combined with one or more other features. Information theory is mainly based on the entropy of a feature, X. The mutual information (MI; Brown et al. 2012) that measures the amount of information between the input feature X and the true class label Y is defined as

$$I(X;Y) = H(X) - H(X \mid Y), \tag{2}$$

where $H(X)$ is the entropy and $H(X\|Y)$ is the conditional entropy. The conditional probability represents the amount of uncertainty remaining in X, after knowing Y. Hence, the mutual information is indicative of the amount of uncertainty in X that is removed by knowing Y. MI can be zero if and only if X and Y are statistically independent. Therefore, it is useful for features to have high MI. A high MI indicates that a feature is correlated with the target variable, and thus can in principle be used by a classifier to yield accurate classifications.

The MI value of the seven features is listed in Table 2. Using the MI method, we are able to choose the features that best describe the difference between two types of classes. However, the selected features might have redundant information, for example two features that give high MI might have the same information, in which a single selected feature could be all that is required to achieve the same classification results.

Table 3. A summary of the performance results of the various classifiers, ordered from best performing to worst performing based on the balanced accuracy and G-mean for binary classification. Two values are given for all metrics. For each binary case presented, the first values represent metric values for Type 1 (RRab) and Type 9 (δ Scuti). The second values are the metrics values for Type 6 (EA) and Type 10 (ACEP). In addition, the average of those metrics are summarized in single value.

Classifiers	Precision	Recall	F1-score	G-mean	Balanced accuracy
			Type 1 (RRab) and Type 6 (EA) classification		
RF	0.97/0.97	0.97/0.97	0.97/0.97	0.97/0.97	0.94/0.94
	∼0.97	∼0.97	∼0.97	∼0.97	∼0.94
DT	0.96/0.96	0.96/0.96	0.96/0.96	0.96/0.96	0.92/0.92
	∼0.96	∼0.96	∼0.96	∼0.96	∼0.92
*K*NN	0.95/0.97	0.97/0.95	0.96/0.96	0.96/0.96	0.92/0.91
	∼0.96	∼0.96	∼0.96	∼0.96	∼0.92
			Type 9 (δ Scuti) and Type 10 (ACEP) classification		
RF	1.0/1.0	1.0/1.0	1.0/1.0	1.0/1.0	1.0/1.0
	∼1.0	∼1.0	∼1.0	∼1.0	∼1.0
DT	1.00/0.96	0.96/1.00	0.98/0.98	0.98/0.98	0.95/0.96
	∼0.98	∼0.98	∼0.98	∼0.98	∼0.96
*K*NN	0.98/0.98	0.96/0.98	0.97/0.97	0.97/0.97	0.93/0.94
	∼0.97	∼0.97	∼0.97	∼0.97	∼0.93

Therefore, a ranking system can be applied, which is also known as the joint mutual information (JMI; Yang & Fong 2011) criterion. The JMI enables the detection of complimentary information, and thereby a reduction in the number of features by eliminating redundancy. The JMI performs a selection from a sample of feature sets based on the amount of complementary information and ranks them. It starts from the feature that possesses the largest MI value, X^1. A greedy iterative process is used to decide which features complement X^1 (Guyon & Elisseeff 2003). The JMI score is given by

$$\mathrm{JMI}\left(X^J\right) = \sum_{X^K \in F} I\left(X^J X^K; Y\right), \tag{3}$$

where $X^J X^K$ is the joint probability of two features and F is the selected features. The iterative process continues until a set of features is selected or all features are ranked. The use of the JMI enables a reduction in the amount of redundancy within the features.

We have applied the JMI to our feature data as shown in Table 2. We note that features that appear to be of low information content, as determined via visual analysis and study using the point biserial correlation coefficient, now appear to be useful. It is tempting to write off features that show low scoring linear correlations. However, it can be seen that even though the period, T, exhibits a low linear correlation, it is ranked as the '1st' best feature by the JMI. Given that we have shown that all the seven features have utility, we apply them all for binary classification.

6.4 Performance of binary classification

For binary classification, we train three classifiers independently using roughly balanced pairwise class combinations from the large-sample and small-sample data sets. We present the results for (i) Type 1: RRab and Type 6: EA and (ii) Type 9: δ Scuti and Type 10: ACEP only to show the difference between utilizing the two different sized data sets. Similar results are obtained with other pairwise combinations of binary classes achieving balanced accuracy and G-mean values that vary by $\sim\pm0.03$.

We found that the RF performs best with an overall balanced accuracy of 0.94 with a G-mean value of 0.97 for Type 1: RRab and Type 6: EA. In addition, we observe that the two science classes in the small data set samples (Type 9: δ Scuti and Type 10: ACEP) have some level of misclassification in multiclass classification, while in the case of binary classification, the RF (being the best performing algorithm) outputs a balanced accuracy of 1.0 with a G-mean value of 1.0. The results for both cases studied are summarized in Table 3.

As discussed in Section 5.3, multiclass classification gave undesirable results. On the other hand, using binary classification (Section 6.4) we show how to obtain improved balanced-accuracies for the science classes, achieving balanced-accuracies >90 per cent in all cases we investigated. We thus now attempt to build upon the result by following a hierarchical approach to classification that will allow us to break the problem into sets of binary comparisons or smaller multiclass comparisons.

7 HIERARCHICAL CLASSIFICATION – RESULTS AND DISCUSSION

Using some astrophysical properties of the variable stars in our data set, we group the variable sources into categories as shown in Fig. 8. The first level of the hierarchy is split into three broad science classes: eclipsing, rotational, and pulsating. From the top level, we continue to subdivide the classes, for instance, at the third level, we are left with exactly two main classes: RR Lyrae and Cepheids with six science subclasses in the final subnode. For further details on hierarchical classification, we refer the reader to the excellent review by Silla & Freitas (2011).

First, we perform a multiclass classification on the first hierarchy layer to distinguish between eclipsing, rotational, and pulsating stars. This method helps to address some of the class imbalance issues. However, this separation is not perfect because the rotational class has many less examples than the other two classes. The same evaluation methodology as in Section 4 is employed and the results for the top layer are summarized in Table 4. We obtain a balanced-

Table 4. A summary of the performance results of the RF classifier for the variable star hierarchical classification. We report metrics per class, separated by '/'. Also, we compute the average metrics taking into consideration the overall classes, summarized in a single value.

Precision	Recall	F1-score	G-mean	Balanced accuracy
		First level: eclipsing, rotational, and pulsating classification		
0.97/0.19/0.51	0.66/0.74/0.87	0.79/0.30/0.64	0.78/0.78/0.86	0.59/0.60/0.75
∼0.86	∼0.70	∼0.74	∼0.79	∼0.61
		Second level: RR Lyrae, LPV, Cepheids, and δ Scuti		
1.00/1.00/0.75/0.96	0.99/0.99/0.95/1.00	0.99/1.00/0.84/0.98	0.99/1.00/0.97/1.00	0.98/0.99/0.93/1.00
∼0.99	∼0.99	∼0.99	∼0.99	∼0.98
		Second level: Ecl and EA		
0.90/0.50	0.92/0.94	0.95/0.65	0.93/0.93	0.86/0.86
∼0.95	∼0.92	∼0.93	∼0.93	∼0.86
		Third level: RRab, RRc, RRd, and Blazhko		
0.96/0.93/0.36/0.29	0.98/0.90/0.44/0.19	0.97/0.91/0.40/0.23	0.97/0.92/0.65/0.44	0.94/0.85/0.40/0.18
∼0.90	∼0.90	∼0.90	∼0.92	∼0.86
		Third level: ACEP and Cep-II		
0.86/0.95	0.96/0.85	0.91/0.90	0.90/0.90	0.82/0.80
∼0.91	∼0.90	∼0.90	∼0.90	∼0.81

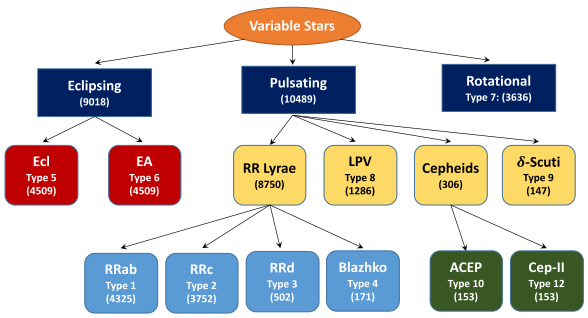

Figure 8. A hierarchy of variable star classification for data used in Section 2 that is constructed based on the understanding of their physical properties. At the top layer, the variable stars can be split into three major classes: eclipsing, rotational, and pulsating systems. The number in parenthesis represents the number of samples in each particular class.

accuracy rate of ∼61 per cent with a G-mean value of ∼0.79 for the first layer.

We then move down the hierarchy to perform two separate classifications for layer 2, keeping the same examples in the training sets and the test sets as in the top layer. We subdivide the eclipsing binary group into Ecl and EA classes and perform a binary classification. The result of this experiment shows that we are successful in classifying between the two classes of objects with a 0.86 balanced accuracy and 0.93 G-mean value. In the second layer, we undertake a multiclass classification of four distinct types of classes: RR Lyrae, LPV, Cepheids, and δ Scuti. We achieve a balanced accuracy of 0.98 in distinguishing between those classes.

Eventually, we follow the hierarchy down to the third layer where we investigate the categorization of two classes: RR Lyrae and Cepheids. Our aim here is to find to what extent we will be successful in distinguishing between the subclasses of RR Lyrae (RRab, RRc, RRd, and Blazhko) and Cepheids (ACEP and Cep-II). The analysis shows that we are successful in distinguishing between RRab and RRc with high balanced accuracy. However, most of the RRd sources are classified as RRc and Blazhko sources are classified as RRab. To check whether our results are affected by class imbalance, we downsample RRc in the training set to the same number of samples as RRd and perform a binary classification. This process is repeated for RRab, whereby the number of objects is decreased to the same number as in Blazhko class. We train a binary classifier, keeping the test set the same for RRc and RRd and RRab and Blazhko. We found that using balanced classes does increase the performance of the classifier significantly, for instance, we are able to distinguish between RRab and Blazhko and RRc and RRd with a balanced-accuracy rate of 80 and 75 per cent, respectively.

For an in-depth analysis of the RR Lyrae subclassification, we use the data provided by Drake et al. (2017) that utilized the adaptive Fourier decomposition (AFD) method (Torrealba et al. 2015) to determine the period of each source. To see how the visually selected periodic variables differ from the initial candidates, we plot the amplitude and the period distribution of the variable stars available in the catalogue. From Fig. 9, we note that it is a challenging task to separate the subclasses: RRab and Blazhko and RRc and RRd. We found that our ML classifier also struggles to separate those classes. In addition, we observe a clear separation between RRab and RRc, and our classification pipeline is also able to separate these two classes. In the same vein, Malz et al. (2018) point out it is generally challenging to have a clear separation between RRc and RRd even though they have different pulsating modes and due to the rarity of RRd sources, they are often subsumed by RRc labels. Moreover, Drake et al. (2017) argued that RRd phased light curves often appear like those of RRc and Blazhko stars often resemble RRab's when phase folded over multiple cycles.

Furthermore, we analyse the classification of Cepheids and we obtain an error classification rate of ∼19 per cent. On the same note, Drake et al. (2017) argued that classifying ACEP and BL Her (a subgroups of Cep-II) is difficult for field stars because of the mixture of stellar populations in the field and the inadequate distance information.

For our hierarchical model, we present the RF classifier results only as it performs well compared to other classifiers discussed in this paper. From the results in Table 4 and Fig. 10, we see immediately a disparity in performance among the classes. This discrepancy in misclassification is due to the comparative size of each of the science classes. We note that we obtain high performance with classes that are data rich. To alleviate the class-

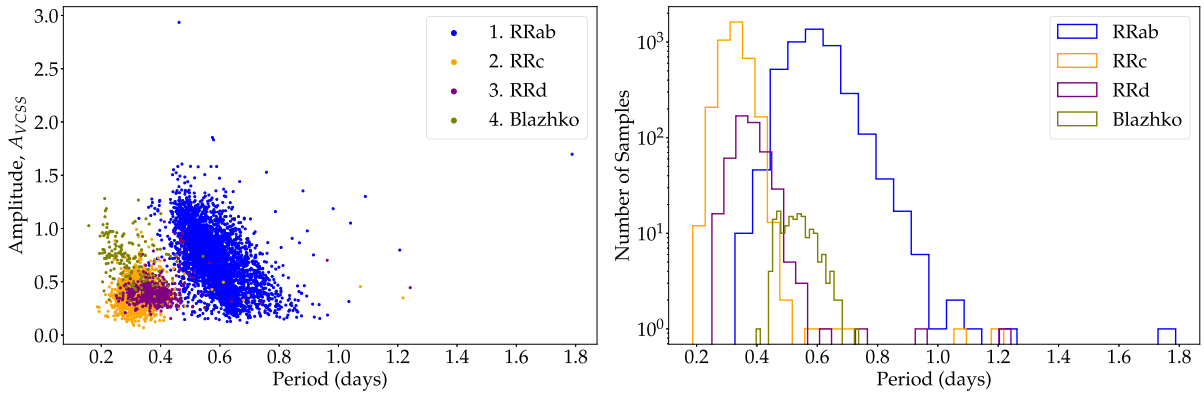

(a) The period-amplitude distribution (b) The period distribution

Figure 9. We plot the distribution of RR Lyrae subtypes (RRab, RRc, RRd, and Blazhko) using available data from the ascii catalogue of the sources in Drake et al. (2017).

Table 5. Comparison of our hierarchical model, multiclass model, and UPSILON package (Kim & Bailer-Jones 2016). For a fair comparison, we test these models on eight classes and report the scores in terms of recall and F1-score. The model with higher classification score shown in bold.

Types of variable stars	UPSILON model with 16 features		Our multiclass model with 7 features		Our hierarchical model with 7 features	
	Recall	F1-score	Recall	F1-score	Recall	F1-score
RRab	0.75	0.86	0.92	0.73	**0.98**	**0.97**
RRc	0.78	0.87	0.77	0.46	**0.90**	**0.91**
RRd	0.11	0.20	0.33	0.14	**0.44**	**0.40**
Ecl (EC and ESD)	0.75	0.73	0.60	0.74	**0.92**	**0.95**
EA	**0.97**	**0.98**	0.90	0.68	0.94	0.65
LPV	0.92	0.96	0.98	0.95	**0.99**	**1.00**
δ Scuti	0.86	0.93	0.96	0.70	**1.00**	**0.98**
Cep-II	0.38	0.55	0.52	0.32	**0.85**	**0.90**

imbalance problem, one can either gather different catalogues for the undersampled classes or augment the existing available catalogues via sophisticated statistical ML approaches.

In Fig. 11, we plot the precision–recall curve for each class and we note that the classification performance is very good. The area under the precision–recall curve values are greater than 0.85 for several classes, except for Type 7: rotational, Type 3: RRd, and Type 4: Blazhko. This correlates with the results presented in Table 4. In addition, we compare our proposed hierarchical approach to an already implemented ML package known as UPSILON (Kim & Bailer-Jones 2016). The latter used a RF classifier, trained on 16 features extracted from the Optical Gravitational Lensing Experiment (OGLE; Udalski, Kubiak & Szymanski 1997) and EROS-2 (Tisserand et al. 2007) periodic variable stars light curves; while our model is trained on seven features from CRTS data. The comparison is made with only eight classes out of 11 as UPSILON has not been trained on all the variable stars available in CRTS data. We report the results in terms of recall and F1-score in Table 5. It is seen that our hierarchical model outperforms the UPSILON model in classifying most of the variable stars, except for Type 6: EA. We can plausibly say that our hierarchical classifier yields good performance with seven features in classifying subgroups of stars as compared to the UPSILON package. For a comparison in terms of features used, we report results when using a 'flat' multiclass model (RF) in Section 5.3 with seven features and compare it with the hierarchical model. The hierarchical model outperforms both the UPSILON model and the multiclass model developed in this paper. This clearly shows that it is not necessary to extract many features to obtain higher classification metrics. In addition, we have shown that converting a 'flat' multiclass problem into a hierarchical system improves variable star classification.

8 CONCLUSION AND FUTURE WORK

With the upcoming synoptic surveys (e.g. LSST; Ivezic et al. 2008), automated transient/variable star classification is becoming an increasingly important field in astronomy. It presents a difficult computational challenge that we have none the less attempted to tackle in this work. We describe the core challenges associated with automatic variable star classification and subsequently explored the nature of the data to be processed. We then applied various approaches with the aim of accurately classifying 11 types of variable star. Some of the methods we applied are similar to current techniques, while others are new to this field. Compared to other related work, we utilized only seven input features during classification, where six features are based on statistical properties of the unfolded data and the period, T, is obtained directly from the data catalogue. We used these features as inputs to three separate commonly employed ML algorithms. We demonstrate that the RF classification algorithm performed best in all test cases. Treating the variable star classification as a multiclass problem with 11 classes, results in a poor performance. In doing so, the RF algorithm is efficient at identifying RRab, RRc, Ecl, EA, rotational, and LPV classes, but is unsuccessful in distinguishing, for example, δ Scuti

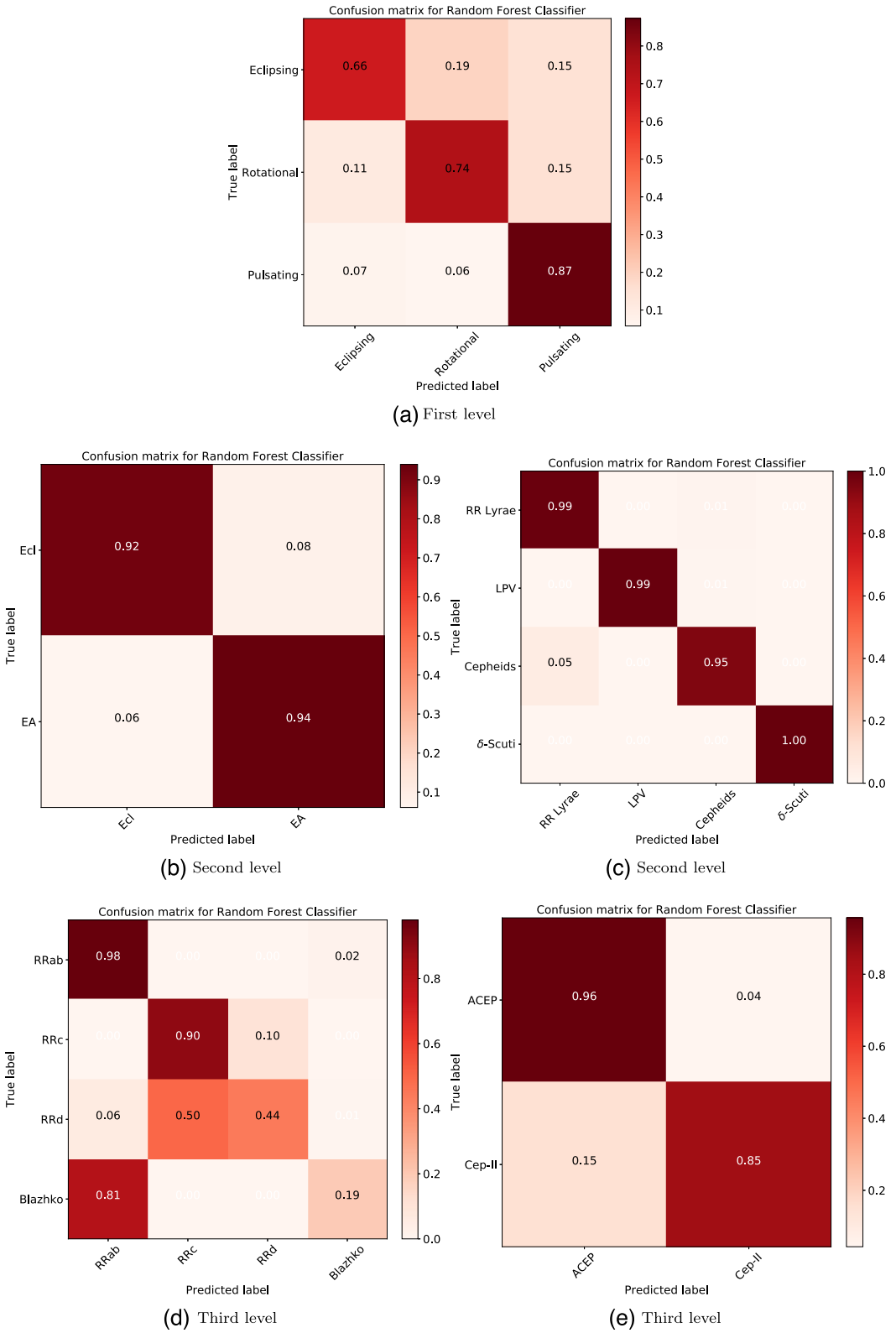

Figure 10. The normalized confusion matrices for the best classifier (RF) for hierarchical classification.

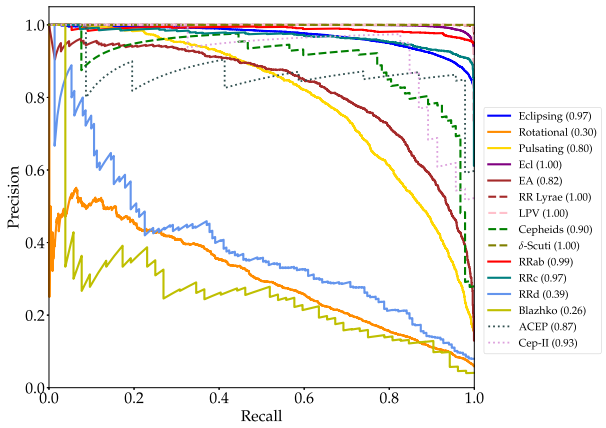

Figure 11. Precision–recall curves for each node in the hierarchical model. Each curve represents a different variable stars with the area under the precision–recall curves score in brackets. This metric is computed on the 30 per cent of the data set used for testing, except that Type 5: Ecl stars has ∼15 647 samples.

and ACEP. However, by decomposing the multiclass problem into several binary classification problems, we gain a significant improvement in balanced accuracy – with a balanced-accuracy rate of 1.0 for the classification of δ Scuti and ACEP. Our results suggest that decomposing a multiclass problem into several binary classification steps could yield improved results.

We therefore developed a hierarchical approach for classifying the 11 variable star classes in our data, by aggregating those classes that show similarities. We show that a hierarchical taxonomy for n-class objects improves the classification rate. We are now successful in identifying subtypes of Cepheids and eclipsing binaries with a balanced-accuracy rate of 81 and 86 per cent, respectively. Whilst the hierarchical approach does not work well for all classes, this is understandable in cases with high class-imbalances and a lack of training examples.

We have presented an approach to analysing variable star data in such a way that is beneficial to ML feature analysis and extraction. This process yields insights that allow us to obtain improved classification performance. In other words, we have taken a principled approach to feature analysis and design, especially for multiclass problems with a highly imbalanced data sets. We employ new methods for feature selection and evaluation and we show that converting a multiclass problem towards a hierarchical classification scheme helps to reduce the class-imbalance problem and provide a significant improvement for variable stars classification. In the near future, we wish to investigate the impact of data augmentation on the performance of our ML classifiers. Moreover, flagging data (as we did for the 'miscellaneous class') is often undesirable. One school of thought is to treat them as outliers but another might argue that these could perhaps indicate new discoveries. It is a major task with such a classification scheme, since we now have to tackle the problem in an unsupervised way, a topic currently in its infancy.

ACKNOWLEDGEMENTS

We thank the referee for useful comments and suggestions for improving this paper. ZH acknowledges support from the UK Newton Fund as part of the Development in Africa with Radio Astronomy (DARA) Big Data project delivered via the Science and Technology Facilities Council (STFC). BS acknowledges funding from the European Research Council (ERC) under the European Union's Horizon 2020 research and innovation programme (grant agreement No. 694745). AM is supported by the Imperial President's PhD Scholarship.

REFERENCES

Bates S. et al., 2011, MNRAS, 416, 2455
Belokurov V., Evans N. W., Le Du Y., 2003, MNRAS, 341, 1373
Bentley J. L., 1975, Commun. ACM, 18, 509
Bergstra J., Yamins D., Cox D. D., 2013, in Proceedings of the 12th Python in Science Conference. Jmlr, p. 13
Blazhko S., 1907, Astron. Nachr., 175, 325
Breiman L., 2001, Machine Learning, 45, 5
Brown G., Pocock A., Zhao M.-J., Luján M., 2012, J. Machine Learning Res., 13, 27
Buturovic L. J., 1993, Pattern Recognition, 26, 611
Catelan M., Smith H. A., 2015, in Pulsating Stars. Wiley-VCH, Weinheim
Cauchy A., 1853, C.R. Acad. Sci, 37, 198
Chao C., Liaw A., Breiman L., 2004,in Using Random Forest to Learn Imbalanced Data. University of California, Berkeley, CA
Danjuma K. J., 2015, preprint (arXiv:1504.04646)
Dietterich T. G., 2000, in Lecture Notes in Computer Science, Vol. 1857, Multiple Classifier Systems. Springer-Verlag, Berlin, p. 1
Djorgovski S. G. et al., 2011, preprint (arXiv:1102.5004)
Djorgovski S. G. et al., 2016, Elsevier, 59, 95
Drake A. J. et al., 2009, ApJ, 696, 870
Drake A. J. et al., 2017, MNRAS, 469, 3688
Eyer L., Blake C., 2005, MNRAS, 358, 30
Gregory P. C., Loredo T. J., 1992, ApJ, 398, 146
Gupta S., 1960, Psychometrika, 25, 393
Guyon I., Elisseeff A., 2003, J. Machine Learning Res., 3, 1157
He H., Garcia E. A., 2009, IEEE Trans. Knowledge Data Eng., 21, 1263
Ivezic Z. et al., 2008, AIP Conference Proceedings, 1082, 359
Juric M. et al., 2015, in Lorente N. P. F., Shortridge K., Wayth R., eds, Astronomical Data Analysis Software and Systems XXV. Astron. Soc. Pac., San Francisco, p. 279
Kim D.-W., Bailer-Jones C. A., 2016, A&A, 587, A18
Kullback S., Leibler R. A., 1951, Ann. Math. Stat., 22, 79
Last F., Douzas G., Bacao F., 2017, preprint (arXiv:1711.00837v2)
Lochner M., McEwen J. D., Peiris H. V., Lahav O., Winter M. K., 2016, ApJS, 225, 31
Lomb N. R., 1976, Ap&SS, 39, 447
Lyon R. J., Stappers B. W., Cooper S., Brooke J. M., Knowles J. D., 2016, MNRAS, 459, 1104
Mahabal A. A. et al., 2012, in Griffin R. E., Hanisch R. J., Seaman R. L., eds, Proc. IAU Symp. Vol. 285, New Horizons in Time-Domain Astronomy. Cambridge Univ. Press, Cambridge, p. 355
Mahabal A., Sheth K., Gieseke F., Pai A., Djorgovski S. G., Drake A., Graham M., 2011, IEEE Symp. Ser. Comput. Intelligence, 1
Malz A. et al., 2018, preprint (arXiv:1809.11145)
Narayan G. et al., 2018, ApJS, 236, 9
Nun I., Protopapas P., Sim B., Zhu M., Dave R., Castro N., Pichara K., 2015, peprint (arXiv:1506.00010)
Pearson K., 1895, Proc. R. Soc. Lond., 58, 240
Pedregosa F. et al., 2011, J. Machine Learning Res., 12, 2825
Quinlan J. R., 1986, Machine Learning, 1, 81
Revsbech E. A., Trotta R., van Dyk D. A., 2018, MNRAS, 473, 3969
Richards J. W. et al., 2011, ApJ, 733, 10
Saha A., Vivas A. K., 2017, AJ, 154, 231
Scargle J. D., 1982, ApJ, 263, 835
Silla C. N. J., Freitas A. A., 2011, Data Mining Knowledge Discovery, 22, 31
Tisserand P. et al., 2007, A&A, 469, 387
Torrealba G. et al., 2015, MNRAS, 446, 2251
Udalski A., Kubiak M., Szymanski M., 1997, Acta Astron., 47, 319
van der Maaten L., Hinton G., 2008, J. Machine Learning Res., 9, 2579

Wattenberg M., Fernanda V., Johnson I., 2016, Distill, http://doi.org/10.23915/distill.00002
Willemsen P. G., Eyer L., 2007, preprint (arXiv:0712.2898)
Yang H., Fong S., 2011, in Cuzzocrea A., Dayal U., eds, Proceedings of the 13th International Conference on Data Warehousing and Knowledge Discovery. Springer Nature, Switzerland, p. 471

APPENDIX A: EVALUATION METRICS

The performance of any ML algorithm is evaluated using measures such as the balanced accuracy, the precision, the recall, the F1-score, sensitivity, and specificity (Chao, Liaw & Breiman 2004). They are defined in terms of true positive (T_P) rate, false positive (F_P) rate, true negative (T_N) rate, and false negative (F_N) Rate. The sensitivity metric is defined as the true positive rate or positive class accuracy, while specificity is referred to as the true negative rate or equivalently negative class accuracy (Danjuma 2015).

(i) Sensitivity measure: equation (A1) also known as the true positive rate or 'recall'. It measures the proportion of actual positives correctly identified by the model:

$$\text{sensitivity/recall} = \frac{T_P}{T_P + F_N}. \tag{A1}$$

(ii) Specificity measure: equation (A2) also known as true negative rate. It measures how well a model identifies negative results:

$$\text{specificity} = \frac{T_N}{T_N + F_P}. \tag{A2}$$

(iii) Precision: it is a measure of retrieved instances that are correctly labelled. Precision is described in equation (A3):

$$\text{precision} = \frac{T_P}{T_P + F_P}. \tag{A3}$$

(iv) F1-score: it is a metrics that aims to quantify overall performance, expressed in terms of precision and recall as shown in equation (A4):

$$\text{F1-score} = \frac{2 \times \text{precision} \times \text{recall}}{\text{precision} + \text{recall}}. \tag{A4}$$

(v) Balanced accuracy measure: it is defined as the average of recall obtained on each class and it is a metric that deals with imbalanced classes:

$$\text{balanced accuracy} = \frac{\text{sensitivity} + \text{specificity}}{2} \times 100\,\text{per cent}. \tag{A5}$$

(vi) G-mean score: G-mean is defined as the squared root of the product of classwise sensitivity. It maximizes the accuracy on each class in addition to keep these accuracies balanced:

$$\text{G-mean} = \sqrt{\text{sensitivity} \times \text{specificity}}. \tag{A6}$$

(vii) Precision–recall (PR) curve: PR curve illustrates the trade-off between true positive rate and positive predictive value for a model at different probability thresholds.

(viii) Confusion matrices: the T_P, F_P, T_N, and F_N can be visualized by a confusion matrix as illustrated in Table A1, where the predicted class is indicated in each column and the actual class in each row. In this case, from Table A1, the true positives (T_P) are Class I examples that were correctly classified as Class I, false positives F_P correspond to Class II examples wrongly classified as Class I. In a similar way, false negatives F_N and true negatives T_N can be explained. For binary classification problems, Class I corresponds to positive class and Class II corresponds to negative class. After the training and testing process, we evaluate our pipeline using balanced accuracy, G-mean, F1-score, recall values, and confusion matrices.

Table A1. Confusion matrix implemented for our specific problem, where the positive class corresponds to Class I and the negative class to Class II for the two classification schemes. True/false positives/negatives are represented as T_P, F_P, T_N, and F_N, respectively.

		Class II	Class I
Actual class	Class II	T_N	F_P
	Class I	F_N	T_P
		Predicted class	

This paper has been typeset from a TEX/LATEX file prepared by the author.